Inorg. Chem. **2007**, *46*, 8652–8661

Synthesis, Structural Characterization, and Biological Studies of New Antimony(III) Complexes with Thiones. The Influence of the Solvent on the Geometry of the Complexes

Ibrahim I. Ozturk,[†] Sotiris K. Hadjikakou,*[,†] Nick Hadjiliadis,*[,†] Nikolaos Kourkoumelis,[†] Maciej Kubicki,[‡] Martin Baril,[§] Ian S. Butler,[§] and Jan Balzarini[||]

Section of Inorganic and Analytical Chemistry, Department of Chemistry, University of Ioannina, 45110 Ioannina, Greece, Faculty of Chemistry, Adam Mickiewicz University, Grunwaldzka 6, 60-780 Poznań, Poland, Department of Chemistry, McGill University, 801 Sherbrooke, Montreal, Quebec H2A 2K6, Canada, and Rega Institute for Medical Research, Katholieke Universiteit Leuven, Minderbroedersstraat 10, B-3000 Leuven, Belgium

Received April 20, 2007

Five new antimony(III) complexes with the heterocyclic thiones 2-mercapto-benzimidazole (MBZIM), 5-ethoxy-2-mercapto-benzimidazole (EtMBZIM), and 2-mercapto-thiazolidine (MTZD) of formulas $\{[SbCl_2(MBZIM)_4]^+\cdot Cl^-\cdot 2H_2O\cdot(CH_3OH)\}$ (**1**), $\{[SbCl_2(MBZIM)_4]^+\cdot Cl^-\cdot 3H_2O\cdot(CH_3CN)\}$ (**2**), $[SbCl_3(MBZIM)_2]$ (**3**), $[SbCl_3(EtMBZIM)_2]$ (**4**), and $[SbCl_3(MTZD)_2]$ (**5**) have been synthesized and characterized by elemental analysis, FT-IR, far-FT-IR, differential thermal analysis–thermogravimetry, X-ray diffraction, and conductivity measurements. Complex $\{[SbCl_2(tHPMT)_2]^+Cl^-\}$, (tHPMT = 2-mercapto-3,4,5,6-tetrahydro-pyrimidine), already known, was also prepared, and its X-ray crystal structure was solved. It is shown that the complex is better described as $\{[SbCl_3(tHPMT)_2]\}$ (**6**). Crystal structures of all other complexes (**1**–**5**) have also been determined by X-ray diffraction at ambient conditions. The crystal structure of the hydrated ligand, EtMBZIM·H_2O is also reported. Compound $[C_{28}H_{24}Cl_2N_8S_4Sb\cdot 2H_2O\cdot Cl\cdot(CH_3OH)]$ (**1**) crystallizes in space group $P2_1$, with $a = 7.7398(8)$ Å, $b = 16.724(3)$ Å, $c = 13.717(2)$ Å, $\beta = 98.632(11)°$, and $Z = 2$. Complex $[C_{28}H_{24}Cl_2N_8S_4Sb\cdot Cl\cdot 3H_2O\cdot(CH_3CN)]$ (**2**) corresponds to space group $P2_1$, with $a = 7.8216(8)$ Å, $b = 16.7426(17)$ Å, $c = 13.9375(16)$ Å, $\beta = 99.218(10)°$, and $Z = 2$. In both **1** and **2** complexes, four sulfur atoms from thione ligands and two chloride ions form an octahedral (Oh) cationic $[SbS_4Cl_2]^+$ complex ion, where chlorides lie at axial positions. A third chloride counteranion neutralizes it. Complexes **1** and **2** are the first examples of antimony(III) compounds with positively charged Oh geometries. Compound $[C_{14}H_{12}Cl_3N_4S_2Sb]$ (**3**) crystallizes in space group $P\bar{1}$, with $a = 7.3034(5)$ Å, $b = 11.2277(7)$ Å, $c = 12.0172(8)$ Å, $\alpha = 76.772(5)°$, $\beta = 77.101(6)°$, $\gamma = 87.450(5)°$, and $Z = 2$. Complex $[C_{18}H_{20}Cl_3N_4O_2S_2Sb]$ (**4**) crystallizes in space group $P\bar{1}$, with $a = 8.6682(6)$ Å, $b = 10.6005(7)$ Å, $c = 13.0177(9)$ Å, $\alpha = 84.181(6)°$, $\beta = 79.358(6)°$, $\gamma = 84.882(6)°$, and $Z = 2$, while complex $[C_6H_{10}Cl_3N_2S_4Sb]$ (**5**) in space group $P2_1/c$ shows $a = 8.3659(10)$ Å, $b = 14.8323(19)$ Å, $c = 12.0218(13)$ Å, $\beta = 99.660(12)°$, and $Z = 4$ and complex $[C_8H_{16}Cl_3N_4S_2Sb]$ (**6**) in space group $P\bar{1}$ shows $a = 7.4975(6)$ Å, $b = 10.3220(7)$ Å, $c = 12.1094(11)$ Å, $\alpha = 71.411(7)°$, $\beta = 84.244(7)°$, $\gamma = 73.588(6)°$, and $Z = 2$. Crystals of complexes **3**–**6** grown from acetonitrile solutions adopt a square-pyramidal (SP) geometry, with two sulfur atoms from thione ligands and three chloride anions around Sb(III). The equatorial plane is formed by two sulfur and two chloride atoms in complexes **3**–**5**, in a *cis*-S, *cis*-Cl arrangement in **3** and **5** and a *trans*-S, *trans*-Cl arrangement in **4**. Finally, in the case of **6**, the equatorial plane is formed by three chloride ions and one sulfur from the thione ligand while the second sulfur atom takes an axial position leading to a unique SP conformation. The complexes showed a moderate cytostatic activity against tumor cell lines.

1. Introduction

Antimonials, such as sodium stibogluconate (Pentostam) and meglumine antimonite (Glucantime), have been widely used for several decades for the treatment of leishmaniasis, a parasitic infection caused by various species of the protozoan *Leishmania*.[1−5] Although the mechanism of action

* To whom correspondence should be addressed. E-mail: shadjika@uoi.gr (S.K.H.), nhadjis@uoi.gr (N.H.). Tel: xx30-26510-98374 (S.K.H.), xx30-26510-98420 (N.H.).
[†] University of Ioannina.
[‡] Adam Mickiewicz University.
[§] McGill University.
[||] Katholieke Universiteit Leuven.

(1) (a) Yan, S.; Lan, L.; Sun, H. In *Metallotherapeutic Drugs and Metal-Based Diagnostic Agents—The Use of Metals in Medicine*; Gielen, M., Tiekink, E. R. T., Eds.; Wiley: Chichester, U.K., 2005. (b) Martindale, *The Extra Pharmacopoeia*, 28th ed.; The Pharmaceutical Press: London, 1982. (c) Marsden, P. D. *Rev. Soc. Bras. Med. Trop.* **1985**, *18*, 187−198.
(2) Tiekink, E. R. T. *Crit. Rev. Onc. Hematol.* **2002**, *42*, 217−224.

10.1021/ic700756e CCC: $37.00
Published on Web 09/13/2007

of these drugs is still unknown, it has been proposed[4−5] that the anti-leishmanial activity of Sb(V) compounds depends on its reduction to Sb(III) inside parasites by the tripeptide of glutathione (GSH, γ-l-Glu-l-Cys-Gly) or by trypanothione [$T(SH)_2$] (a conjugation of glutathione and the polyamine spermine, i.e., N^1,N^8-bis(glutathionyl)spermidine).[1a,4−6] This redox behavior of the metal center is found to affect the geometry of the core of the complex[7] while the geometry transformations, which may take place during this process, may involve (i) the intermolecular interactions, which play an important role in the solid-state arrangement, (ii) the solvation effects, and (iii) the $5s^2$ lone pair of electrons located on Sb(III), as well.[7] As the anti-leishmanial activity of Sb(V) has been found to depend on its reduction to Sb(III) inside parasites,[3,6] it is of importance to investigate the direct influence of Sb(III). Thus, the thiones, a well-known class of reductant ligands, were used to prepare stable Sb(III)−thione complexes. There are few reports in the literature referring to the structural characterization of antimony(III) complexes with thiones.[8−12] Taking into account both the primary and/or the secondary interactions around the antimony(III) cation, Sb(III)−thione complexes were found, thus far, to adopt pseudotrigonal-bipyramidal (ψ-TBP), trigonal-pyramidal (TP), square-pyramidal (SP), octahedral (Oh), and pentagonal-pyramidal (PP) geometries (Scheme 1).

Antitumor properties and the cytotoxicity of antimony(III) and antimony(V) compounds have also been reported

Scheme 1

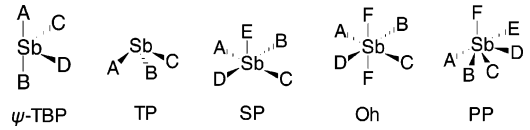

and reviewed recently by Edward Tiekink.[2] The most-studied antimony(III) compounds in the context of antitumor activity are organometallics such as diphenylantimony(III) thiolates, i.e., $[Ph_2Sb(S_2PPh_2)]$ and $[Ph_2Sb(S_2P(O^iPr)_2]$.[2]

Thus, the study of the structural behavior of the complexes derived from the reaction between antimony(III) halides and thiones is a matter of significant importance, both for the investigation of the geometries of the compounds and the factors influencing them and for their use as medicinal drugs[1−3,13] or in catalytic processes.[13]

In this paper, we report the structural and spectroscopic characterization of five new antimony(III) trichloride complexes with the heterocyclic thiones 2-mercapto-benzimidazole (MBZIM), 5-ethoxy-2-mercapto-benzimidazole (EtMBZIM), and 2-mercapto-thiazolidine (MTZD) of formulas $\{[SbCl_2(MBZIM)_4]^+\cdot Cl^-\cdot 2H_2O\cdot(CH_3OH)\}$ (**1**), $\{[SbCl_2(MBZIM)_4]^+\cdot Cl^-\cdot 3H_2O\cdot(CH_3CN)\}$ (**2**), $[SbCl_3(MBZIM)_2]$ (**3**), $[SbCl_3(EtMBZIM)_2]$ (**4**), and $[SbCl_3(MTZD)_2]$ (**5**) that show an interesting structural diversity. The already-known complex $\{[SbCl_2(tHPMT)_2]^+Cl^-\}$[8e], which is now better described as a neutral $\{[SbCl_3(tHPMT)_2]\}$ (**6**) (tHPMT = 2-mercapto-3,4,5,6-tetrahydro-pyrimidine) species, was also prepared under the same conditions with complexes **1**−**5** and characterized by X-rays, for comparison.

It is found that the presence of water as a solvent and ligand greatly influences the geometry of the complexes around Sb(III).

2. Results and Discussion

I. General Aspects. Antimony(III) complexes **1**−**6** have been synthesized by reacting the appropriate thione with an excess of antimony(III) trichloride $SbCl_3$ in dichloromethane/methanolic or dichlortomethane/acetonitrile solutions, as shown by the following equations.

$$SbCl_3 + 4MBZIM \xrightarrow[MeOH\ or\ MeCN/H_2O]{CH_2Cl_2} \{[Sb(MBZIM)_4Cl_2]^+Cl^-(solv)\}$$

where solv = $2H_2O\cdot MeOH$ (**1**) and $3H_2O\cdot MeCN$ (**2**).

$$SbCl_3 + 2HL \xrightarrow[CH_3CN]{CH_2Cl_2} [Sb(HL)_2Cl_3]$$

where HL = MBZIM (**3**), EtMBZIM (**4**), MTZD (**5**), and tHPMT (**6**).

All complexes are air-stable powders. Crystals of compounds **1**−**6**, suitable for X-ray analysis, were grown by slow evaporation of the solvents.

(3) Yan, S.; Li, F.; Ding, K.; Sun, H. *J. Biol. Inorg. Chem.* **2003**, *8*, 689−697.
(4) Guo, Z.; Sadler, P. J. *Adv. Inorg. Chem.* **2000**, *49*, 183−306.
(5) Sun, H.; Yan, S. C.; Cheng, W. S. *Eur. J. Biochem.* **2000**, *267*, 5450−5457.
(6) Shaked-Mishan, P.; Ulrich, N.; Ephros, M.; Zilberstein, D. *J. Biol. Chem.* **2001**, *276*, 3971−3976.
(7) Avarvari, N.; Faulques, E.; Fourmigue, M. *Inorg. Chem.* **2001**, *40*, 2570−2577.
(8) (a) Hough, E.; Nicholson, D. G. *J. Chem. Soc., Dalton Trans.* **1981**, 2083−2087. (b) Rubin, B.; Heldrich, F. J.; Dean, W. K.; Williams, D. J.; Viehbeck, A. *Inorg. Chem.* **1981**, *20*, 4434−4437. (c) Fisher, R. A.; Nielsen, R. B.; Davis, W. M.; Buchwald, S. L. *J. Am. Chem. Soc.* **1991**, *113*, 165−171. (d) Doidge-Harrison, S. M. S. V.; Irvine, J. T. S.; Spencer, G. M.; Wardell, J. L.; Wei, M.; Ganis, P.; Valle, G. *Inorg. Chem.* **1995**, *34*, 4581−4584. (e) Razak, I-A.; Usman, A.; Fun, H.-K.; Yamin, B. M.; Kea, G.-W. *Acta Crystallogr.* **2002**, *C58*, m122−m123.
(9) (a) Clegg, W.; Elsegood, M. R. J.; Farrugia, L. J.; Lawlor, F. J.; Norman, N. C.; Scott, A. J. *J. Chem. Soc., Dalton Trans.* **1995**, 2129−2135. (b) Bochmann, M.; Song, X.; Hursthouse, M. B.; Karaulov, A. *J. Chem. Soc., Dalton Trans.* **1995**, 1649−1652 and references therein.
(10) (a) Berges, P.; Hinrichs, W.; Kopf, J.; Mandak, D.; Klar, G. *J. Chem. Res.* **1985**, *218*, 2601. (b) Marsh, R. E.; Kapon, M.; Hu, S.; Herbstein, F. H. *Acta Crystallogr., Sect. B: Struct. Sci.* **2002**, *58*, 62. (c) Williams, D. J.; Vanderveer, D.; Jones, R. L.; Menaldino, D. S.; *Inorg. Chim. Acta* **1989**, *165*, 173. (d) Kisenyl, J. M.; Willey, G. R.; Drew, M. G. B. *J. Chem. Soc., Dalton Trans.* **1985**, 1073−1075. (e) Preut, H.; Huber, F.; Hengstmann, K.-H. *Acta Crystallogr.* **1988**, *C44*, 468−469 (f) Hengstmann, K. H.; Huber, F.; Preut, H. *Acta Crystallogr.* **1991**, *C47*, 2029−2032.
(11) (a) Block, E.; Ofori-Okai, G.; Kang, H.; Wu, J.; Zubieta, J. *Inorg. Chem.* **1991**, *30*, 4784−4788. (b) Ganis, P.; Marton, D.; Spencer, G. M.; Wardell, J. L.; Wardell, S. M. S. V. *Inorg. Chim. Acta* 2000, *308*, 139−142. (c) Alan Howie, R.; Low, J. N.; Spencer, G. M.; Wardell, J. L. *Polyhedron* **1997**, *16*, 2563−2571. (d) Spencer, G. M.; Wardell, J. L.; Aupers, J. H. *Polyhedron* **1996**, *16*, 2701−2706.
(12) (a) Hadjikakou, S. K.; Antoniadis, C. D.; Hadjiliadis, N.; Kubicki, M.; Binolis, J.; Karkabounas, S.; Charalabopoulos, K. *Inorg. Chim. Acta* **2005**, *358*, 2861−2866 (b) Bozopoulos, A. P.; Kokkou, S. C.; Rentzeperis, P. J.; Karagiannidis, P. *Acta Crystallogr.* **1984**, *C40*, 944−946.
(13) (a) McAuliffe, C. A. In *Comprehensive Coordination Chemistry*; Wilkinson, G., Gillard, R. D., McCleverty, J. A., Eds.; Pergamon: Oxford, U.K.,1987; Vol. 3. (b) Alonzo, G.; Bertazzi, N.; Consiglio, M. *Inorg. Chim. Acta* **1984**, *85*, L35. (c) Wandiga, S. O. *J. Chem. Soc., Dalton Trans.* **1975**, 1894.

II. Thermal Analysis. Thermal analysis in flowing nitrogen shows that the decomposition of octahedral complex **1** sums up to a total of 83.5% mass loss and it is connected with four endothermic effects. The thermogravimetric analysis (TGA) and differential thermal analysis (DTA) data curves for complex **1** show that the first stage of decomposition (94−120 °C, **1**) is connected with an endothermic effect and involves a 3.4% mass loss of methanol (calculated mass loss 3.6%) The second stage (136−228 °C) is connected with a double endothermic effect and involves a 11.8% mass loss of two water molecules and two chloride ions (calculated mass loss 11.9%). A third decomposition stage (230−450 °C) of 51.0% mass loss corresponds to the loss of three ligands (calculated mass loss 50.2%) followed by a fourth decomposition stage (611−740 °C) which involves 17.6% mass loss of the remaining ligand molecule (the calculated mass loss is 16.7%).

The corresponding thermal analysis of SP complexes **3** and **4** shows a decomposition in two steps which sums up to a total mass loss of 87.3% (**3**) and 81.5% (**4**), respectively. The first stage of decomposition (97−347 °C for **3** and 57−391 °C for **4**) is connected with a multiple endothermic effect and involves a 55.3% (**3**) and 60.5% (**4**) mass loss consistent with the evolution of two ligand molecules of MBZIM for **3** and EtBZIM for **4** (calculated mass losses of 56.8% (**3**) and 62.9% (**4**)). The second stage of decomposition (348−567 °C (**3**) and 397−594 °C (**4**)) is connected with an endothermic effect and involves a 19.4% (**3**) and 16.3% (**4**) mass loss of three chlorines (calculated mass losses of 20.1% (**3**) and 17.3% (**4**)).

The TGA and DTA data curves for complex **5**, which also adopts a SP geometry around Sb(III), also show a two-step decomposition, where the first stage (59−251 °C) is connected with a double endothermic effect and involves a 19.3% mass loss, consistent with the evolution of three chlorine atoms (calculated mass loss 22.8%). The second stage of decomposition (250−344 °C) connected with an endothermic effect involves a 51.4% (**4**) mass loss of three chlorines (calculated mass loss 51.1%).

III. Vibrational Spectroscopy. The IR spectra of complexes **1**−**6** show distinct vibrational bands at 1492 and 1348 cm^{-1} (**1**), 1498 and 1349 cm^{-1} (**2**), 1508 and 1345 cm^{-1} (**3**), 1491 and 1304 cm^{-1} (**4**), 1519 and 1305 cm^{-1} (**5**), and 1577 and 1232 cm^{-1} (**6**), which can be assigned to ν(CN) vibrations (thioamide I and II bands) at 1012 and 753 cm^{-1} (**1**), 1007 and 739 cm^{-1} (**2**), 1013 and 746 cm^{-1} (**3**), 1067 and 823 cm^{-1} (**4**), 993 and 658 cm^{-1} (**5**), and 1074 and 634 cm^{-1} (**6**), which can be attributed to the ν(CS) vibrations (thioamide III and IV bands). The corresponding thioamide bands of the free ligands are found at 1513, 1339, 1016, and 743 cm^{-1} for MBZIM,[14a] 1499, 1307, 1173, and 810 cm^{-1} for EtMBZIM, 1516, 1296, 998, and 667 cm^{-1} for MTZD,[14b] and at 1557, 1206, 1067, and 644 cm^{-1} for tHPMT,[14c] respectively. Amide N−H bond vibrations were observed in the region of 3125−3270 cm^{-1} in complexes **1**−**6**. Bands at 326 and 325 cm^{-1} in the far-IR spectra of complexes **1** and **3** have been assigned to the vibrations of Sb−Cl bonds, while bands at 300 cm^{-1} in **1** and at 290 cm^{-1} in **3** are attributed to the ν(Sb−S) vibrations.[14d] The lower wavenumber in the ν(Sb−S) vibration band (290 cm^{-1}) observed in **3** is in contrast to the corresponding one in **1** (300 cm^{-1}), which is in accordance with the Sb−S bond lengths measured (see crystal structures). Sb−S and Sb−Cl vibrations are also Raman active.[14e,f] Thus, bands at 202, 203, and 212 cm^{-1} in the Raman spectra of complexes **1**, **3**, and **5** are due to the ν(Sb−S) vibration while bands at 317, 318−329, and at 307−320 cm^{-1} are assigned to the ν(Sb−Cl) vibration. It is noteworthy that the presence of two type of Sn−Cl bonds (see crystal structures) in complexes **3** and **5** with SP geometry leads to two distinct vibrations in their Raman spectra (Figure 1).[14e,f]

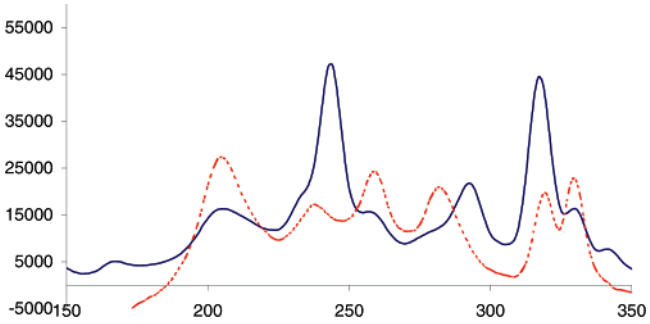

Figure 1. Raman spectra (150−350 cm^{-1}) of complexes (**1**) (—, blue) and (**3**) (- - -, red).

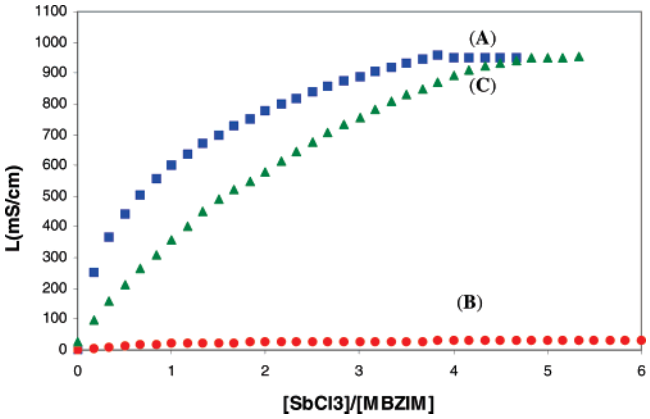

Figure 2. Conductivity titrations of 10^{-2} M MBZIM, with 10^{-1} M $SbCl_3$ in MeOH (A), CH_3CN (B), and CH_3CN/H_2O 5:1 (C) (T = 293 K).

IV. Conductivity Measurements. Since complexes **1** and **2** with octahedral geometries are ionic salts while complexes **3**−**6** are neutral, we investigated the influence of the solvent during their synthesis by studying their conductivity titrations of the ligands,with $SbCl_3$ solutions. Figure 2 shows the conductivity titrations of 10^{-2} M MBZIM, with 10^{-1} M $SbCl_3$ in MeOH (A), CH_3CN (B), and CH_3CN/H_2O 5/1 v/v (C) (T = 293 K).

(14) (a) Daga, V.; Hadjikakou, S. K.; Hadjiliadis, N.; Kubicki, M.; dos Santos, J. H. Z.; Butler, I. S. *Eur. J. Inorg. Chem.* **2002**, 1718−1728. (b) Hadjikakou, S. K.; Xanthopoulou, M. N.; Hadjiliadis, N.; Kubicki, M. *Can. J. Anal. Sci. Spectrosc.* **2003**, *48*, 38−45. (c) Zachariadis, P. C.; Hadjikakou, S. K.; Hadjiliadis, N.; Michaelides, A.; Skoulika, S.; Balzarini, J.; De Clercq, E. *Eur. J. Inorg. Chem.* **2004**, 1420−1426. (d) Drew, M. G. B.; Kisenyi, J. M.; Willey, G. R.; Wandiga, S. O. *J. Chem. Soc., Dalton Trans.* **1984**, 1717−1721. (e) Ludwig, C.; Dolny, M.; Gotze, H.-J. *Spectrochim. Acta, Part A* **2000**, *56*, 547−555. (f) Klapotke, T. M.; Noth, H.; Schutt, T.; Warchold, M. *Z. Anorg. Allg. Chem*. **2001**, *627*, 81−84.

Scheme 2

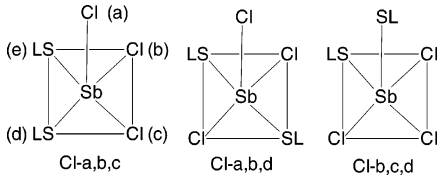

At zero $SbCl_3$ concentration, MBZIM solution (Figure 2) has almost zero conductivity in both methanol or acetonitrile solutions. This increases up to a maximum value when the $[SbCl_3]$/[MBZIM] ratio is increased up to 4:1 in the case of methanol solution. This may be attributed to the formation of an ionic complex **1** in methanol. In the case of acetonitrile solutions, the conductivity remains almost zero in all $[SbCl_3]$/[MBZIM] ratios studied. This could be explained by the formation of the neutral complex **3** in acetonitrile solutions.

In a mixture of water/acetonitrile (1:5) solution, however, the ionic complex **2** was obtained. It therefore seems that water plays a crucial role in determining the geometry of the product obtained. To further support this hypothesis, we studied the conductivity titration of MBZIM by $SbCl_3$ in a mixture of acetonitrile/water solutions in a ratio of 5:1 v/v (Figure 2C). A significant conductivity was now detected (Figure 2C), which increases up to a maximum value when the $[SbCl_3]$/[MBZIM] ratio increases up to 4:1. These results are further supported by the X-ray crystal-structure determinations (see crystal structures). A similar behavior was also found for the reaction between EtMBZIM, MTZD, and tHPMT with $SbCl_3$ in both methanol and acetonitrile solutions. Thus, in the case of titrations of methanolic solutions of EtMBZIM, MTZD, and tHPMT with $SbCl_3$ solutions, the conductivity increases up to a maximum value when the $[SbCl_3]$/[ligand] ratio is increased up to 6:1 in the case of EtMBZIM, 2.5:1 in the case of MTZD, and 4:1 in the case of tHPMT, while in acetonitrile the conductivity remains almost zero in all $[SbCl_3]$/[ligand] ratios studied.

V. Crystal and Molecular Structures of 1−6. Crystal structures of antimony(III) compounds are rare in the literature due to the hydrolysis they undergo in aqueous solutions. Antimony(III)−thione complexes are found to adopt the following geometries: (i) (ψ-TBP) geometry (Scheme 1) as in $SbCl_3$(tmtu) (tmtu = tetramethylthiourea),[8a] $SbCl_3$(dmit) (dmit = 1,3-dimethyl-2-(*3H*)-imidazole-thione),[8b] 1-halo-stibathiolane of 1,2-dimethyl-propanothiolane-3,[8c] 1,2-diphenyl-propanothiolane-3,[8c] or *n*-hehanothiolane-6,[8c] $\{[Sb(1,2\text{-}S_2C_6H_4)_2]^-\}$ (1,2-$S_2C_6H_4$ = benzene-1,2-dithiol), $\{[Sb(dmit)_2]^-\}$ (H_2-dmit = 4,5-dimercapto-1,3-dithiole-2-thione),[8d] and $\{[SbCl_2(tHPMT)_2]^+Cl^-\}$,[8e] better described, however, as a complex with a SP geometry (see crystal structure); (ii) TP geometry (Scheme 1) as in $Sb(SR)_3$ (R−SH = 4-Me-C_6H_4−SH and 3,5-Me_2-C_6H_3−SH)[9a] and $Sb(SR)_3$ (R−SH = HS−C_6H_2-^{i}Pr$_3$-2,4,6);[9b] (iii) SP geometry (Scheme 1) as in $[SbCl_3(NMBZT)_2]$ (NMBZT = *N*-methyl-2-mercapto-benzothiazole),[10a] $[SbCl_3(NMIM)_2]$ (NMIM = *N*-methyl-2-mercapto-imidazole),[10a,b] $[SbCl_3(L)_2]$ (L = 1,1′-methylene-bis(3-methyl-2H-imidazole-2-thione,[10c] $[SbCl_3(C_2H_5NHC(S)CH_2C(S)NHC_2H_5)]$,[10d] [PhSb(dmit)] ($H_2$-dmit = 4,5-dimercapto-1,3-dithiole-2-thione),[7] $[PhSb(pyt)_2]$ (pytH = pyridine-2-thione),[10e] and [mesitylSb(pyt)$_2$];[10f] (iv) Oh geometry (Scheme 1) as in $[Sb(2\text{-}SC_5H_4N)_3]$ and $[Sb(2\text{-}SC_5H_3N\text{-}3\text{-}SiMe_3)_3]$[11a] and $\{[Sb(dmit)_2]^-\}$ (H_2dmit = 4,5-dimercapto-1,3-dithiole-2-thione);[11b−d] and (v) PP geometry (Scheme 1) as in the case of $[Sb(pmt)_3]\cdot 0.5(CH_3OH)$, (pmt = 2-mercapto-pyrimidine)[12a] and $[Sb(2\text{-}SC_5H_4N)_3]$ (2-SC_5H_4N = 2-mercapto-pyridine).[12b]

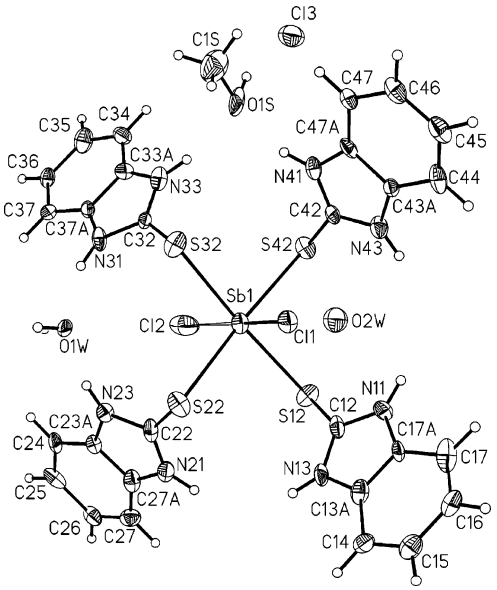

Figure 3. Anisotropic ellipsoid representation of complex **1**. The ellipsoids are drawn at the 50% probability level.

It is noteworthy that stereoisomers may also be found in these type of geometries, increasing the type and number of structural motifs that these compounds may adopt. Therefore, in the case of $SbCl_3L_2$ complexes with SP conformation, three type of stereoisomers can be formed, which are defined by letters indicative of the equivalent positions (Scheme 2), while $\{[SbCl_2L_4]^+\}$ complexes with Oh conformation may form *cis*- or *trans*-Cl stereoisomers.

ORTEP diagrams of the named complexes are shown in Figures 3−8 while selected bond lengths and angles are given in Table 1.

The antimony(III) compounds **1**−**6** are monomeric in the solid state. In both **1** and **2** complexes, four sulfur atoms from thione ligands and two chloride ions form an Oh cationic $[SbS_4Cl_2]^+$ complex, with the chlorides lying at the axial positions. A third chloride serves as a counterion. Complexes **1** and **2** are the first examples of antimony(III) compounds with Oh geometry positively charged. Complexes **3**−**6** were grown from acetonitrile solutions Two sulfur atoms, from thione ligands and three chloride ions, form SP geometries around antimony(III) with a,b,c-Cl $[SbCl_3(MBZIM)_2]$ (**3**), a,b,d-Cl $[SbCl_3(EtMBZIM)_2]$ (**4**), a,b,c-Cl $[SbCl_3(MTZD)_2]$ (**5**), and b,c,d-Cl $[SbCl_3(tHPMT)_2]$ (**6**) conformations (See Scheme 2).

The Sb−S bond distances varied from 2.482 to 2.849 Å (Table 1) in all complexes **1**−**6**, except for one of the two Sb−S bonds of complex **3** found to be longer (3.0085 Å), but still shorter than the sum of the van der Waals radii (4.0 Å).[15] The Sb−Cl bond distances varied from 2.3762 to 3.010 Å (Table 1). Since the sum of the van der Wals radii for

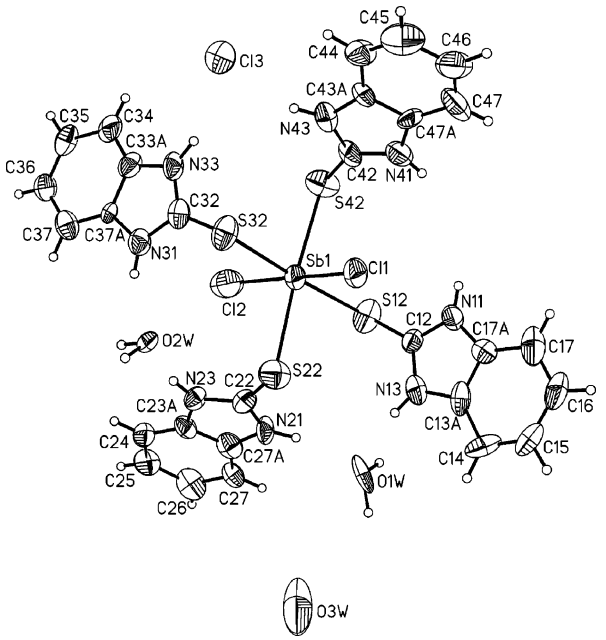

Figure 4. Anisotropic ellipsoid representation of complex **2**. The ellipsoids are drawn at the 50% probability level. The poor quality of the crystals allows only a rough description of the molecular structure of the complex while the solvent molecules were omitted from the figure for clarity.

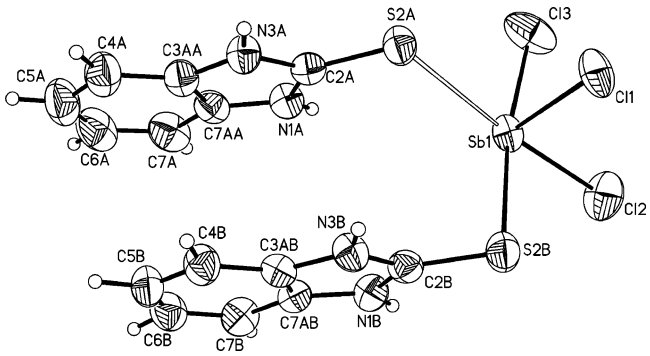

Figure 5. Anisotropic ellipsoid representation of complex **3**. The ellipsoids are drawn at the 50% probability level.

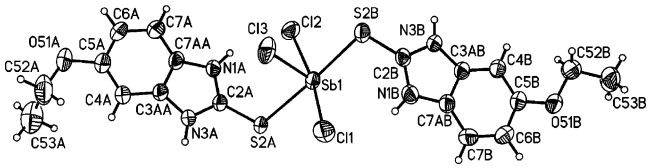

Figure 6. Anisotropic ellipsoid representation of complex **4**. The ellipsoids are drawn at the 50% probability level.

Sb−Cl bonds is 3.95 Å,[15] we consider the Sb−Cl interaction of 3.010 Å found in **1** or 3.006 Å measured in **6** as bonding interactions. The Sb−Cl bond distances found in complexes **1**−**6** are in agreement with those found in $SbCl_3(tmtu)$[8a] (Sb−Cl1 = 2.687(2) Å, Sb−Cl2 = 2.527(3) Å, and Sb−Cl3 = 2.428 Å) and in $SbCl_3(dmit)$[8b] (Sb−Cl1 = 2.532(2) Å and Sb−Cl2 = 2.43191 Å) and Sb−Cl3 = 2.636(1) Å. The Cl−Sb−Cl bond angles are 178.23° for **2** and 178.13° in **1**, indicating a small distortion from the ideal octahedral geometry. The C−S bond lengths varied from 1.686 to 1.725

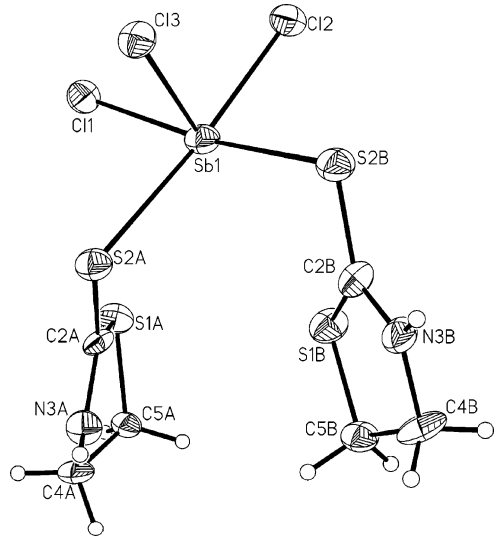

Figure 7. Anisotropic ellipsoid representation of complex **5**. The ellipsoids are drawn at the 50% probability level.

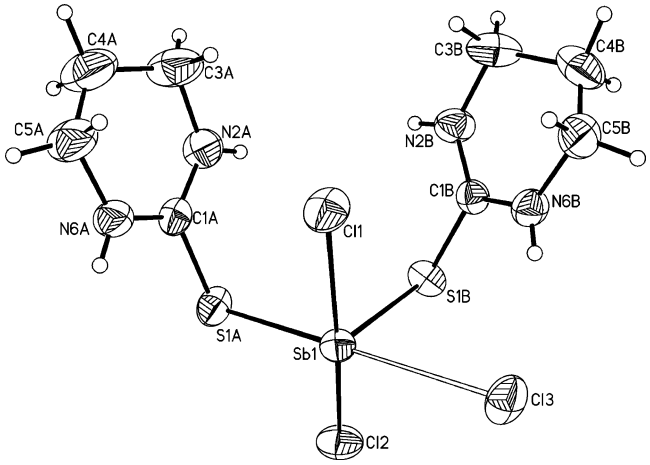

Figure 8. Anisotropic ellipsoid representation of complex **6**. The ellipsoids are drawn at the 50% probability level.

Å in the case of complexes **1**−**3** with the MBZIM ligand confirming the coordination of the ligand with its neutral form (average C−S length = 1.69 Å).[14a,16a] The thionate form is also employed in the ligand of complex **4** (S2A−C2A = 1.716(3) Å and S2B−C2B = 1.707(3) Å, respectively. The C−S bond in free EtMBZIM ligand is 1.691(3) Å in length (see the crystal structure of EtMBZIM). The corresponding C−S bond distances of the ligands MTZD and tHPMT found in complexes **5** and **6** are 1.713(11) and 1.728(13) Å, respectively, in **5** and 1.754(2) and 1.7542(19) Å, respectively, in **6**, which also confirm the neutral form of the coordinated ligands (average C−S length = 1.69 Å for MTZD[14a,b] and average C−S length = 1.74 Å for tHPMT[14c,16b]). The lone pair of electrons located on Sb atoms of complexes **3**−**6** affects the ideal SP geometry around the metal ion[17a] since the basal bond angles are found to vary from the ideal values of 180° or 90° (Table 1) in accordance with

(15) (a) Batsanov, S. S. *Inorg. Mater.* **2001**, *37*, 871−885; translated from *Neorg. Mater.* **2001**, *37*, 1031−1046. (b) Bondi, A. *J. Phys. Chem.* **1964**, *68*, 441−451.

(16) (a) Corban, G. J.; Hadjikakou, S. K.; Hadjiliadis, N.; Kubicki, M.; Tiekink, E. R. T.; Butler, I. S.; Drougas, E.; Kosmas, A. M. *Inorg. Chem.* **2005**, *44*, 8617−8627. (b) Zartilas, S.; Kourkoumelis, N.; Hadjikakou, S. K.; Hadjiliadis, N.; Zachariadis, P.; Kubicki, M.; Denisov, A.-Y.; Butle, I. S. *Eur. J. Inorg. Chem.* **2007**, 1219−1224.

Table 1. Selected Bond Lengths (Å) and Angles (deg) for Triorganotin(IV) Complexes **1**−**6** Measured at r.t. (esd's in Parentheses)

complex **1**		complex **2**		complex **3**		complex **4**	
			(a) bond lengths				
Sb1−Cl1	2.457(3)	Sb1−Cl1	2.464(4)	Sb1−Cl1	2.3827(8)	Sb1−Cl1	2.5169(8)
Sb1−Cl2	3.010	Sb1−Cl2	2.949	Sb1−Cl2	2.4434(10)	Sb1−Cl2	2.7840(8)
Sb1−S12	2.733(3)	Sb1−S12	2.752(4)	Sb1−Cl3	2.6173(12)	Sb1−Cl3	2.3762(8)
Sb1−S22	2.767(4)	Sb1−S22	2.775(4)	Sb1−S2A	3.0085	Sb1−S2A	2.7728(8)
Sb1−S32	2.791(4)	Sb1−S32	2.775(4)	Sb1−S2B	2.7606(9)	Sb1−S2B	2.7285(8)
Sb1−S42	2.759(3)	Sb1−S42	2.763(4)	S2A−C2A	1.698(2)	S2A−C2A	1.716(3)
S12−C12	1.711(12)	S12−C12	1.697(14)	S2B−C2B	1.710(2)	S2B−C2B	1.707(3)
S22−C22	1.692(12)	S22−C22	1.716(16)				
S32−C32	1.711(12)	S32−C32	1.686(14)				
S42−C42	1.725(12)	S42−C42	1.693(15)				
			(b) angles				
Cl1−Sb1−S12	91.50(10)	Cl1−Sb1−S12	91.70(13)	Cl1−Sb1−Cl2	91.80(3)	Cl1−Sb1−Cl2	171.53(3)
Cl1−Sb1−S22	83.51(10)	Cl1−Sb1−S22	82.76(13)	Cl1−Sb1−Cl3	89.08(3)	Cl1−Sb1−Cl3	89.93(3)
Cl1−Sb1−S32	82.85(10)	Cl1−Sb1−S32	83.37(11)	Cl2−Sb1−Cl3	86.83(4)	Cl2−Sb1−Cl3	84.59(3)
Cl1−Sb1−S42	90.69(10)	Cl1−Sb1−S42	92.23(13)	Cl1−Sb1−S2A	78.34	Cl1−Sb1−S2A	88.91(2)
Cl2−Sb1−S12	89.89	Cl2−Sb1−S12	89.40	Cl1−Sb1−S2B	85.23(3)	Cl1−Sb1−S2B	89.64(3)
Cl2−Sb1−S22	95.10	Cl2−Sb1−S22	95.85	Cl2−Sb1−S1A	169.56	Cl2−Sb1−S2A	84.79(2)
Cl2−Sb1−S32	95.80	Cl2−Sb1−S32	95.56	Cl2−Sb1−S2B	88.15(3)	Cl2−Sb1−S2B	96.15(2)
Cl2−Sb1−S42	90.73	Cl2−Sb1−S42	89.17	Cl3−Sb1−S2A	96.33	Cl3−Sb1−S2A	91.47(3)
Cl2−Sb1−Cl1	178.04	Cl2−Sb1−Cl1	178.23	Cl3−Sb1−S2B	172.30(3)	Cl3−Sb1−S2B	83.60(3)
S12−Sb1−S22	90.41(10)	S12−Sb1−S22	90.30(12)	S2A−Sb1−S2B	87.63	S2A−Sb1−S2B	174.86(2)
S12−Sb1−S32	174.17(10)	S12−Sb1−S32	174.92(13)				
S12−Sb1−S42	88.04(9)	S12−Sb1−S42	88.70(12)				
S22−Sb1−S32	90.39(11)	S22−Sb1−S32	90.29(12)				
S22−Sb1−S42	173.96(10)	S22−Sb1−S42	174.87(15)				
S32−Sb1−S42	90.57(10)	S32−Sb1−S42	90.27(12)				

complex **5**		complex **6**	
	(a) bond lengths		
Sb1−Cl1	2.573(3)	Sb1−Cl1	2.5128(6)
Sb1−Cl2	2.481(3)	Sb1−Cl2	2.6670(6)
Sb1−Cl3	2.385(3)	Sb1−Cl3	3.006
Sb1−S2A	2.849(3)	Sb1−S1A	2.5527(7)
Sb1−S2B	2.816(3)	Sb1−S1B	2.4823(6)
S2A−C2A	1.713(11)	S1A−C1A	1.754(2)
S2B−C2B	1.728(13)	S1B−C1B	1.7542(19)
	(b) angles		
Cl1−Sb1−Cl2	90.22(11)	Cl1−Sb1−Cl2	163.58(2)
Cl1−Sb1−Cl3	87.32(11)	Cl1−Sb1−Cl3	90.13
Cl2−Sb1−Cl3	89.65(11)	Cl2−Sb1−Cl3	100.94
Cl1−Sb1−S2A	93.22(10)	Cl1−Sb1−S1A	92.30(2)
Cl1−Sb1−S2B	169.11(11)	Cl1−Sb1−S1B	92.47(2)
Cl2−Sb1−S2A	168.51(11)	Cl2−Sb1−S1A	76.17(2)
Cl2−Sb1−S2B	88.11(10)	Cl2−Sb1−S1B	76.65(2)
Cl3−Sb1−S2A	79.57(10)	Cl3−Sb1−S1A	176.58

the valence-shell electron-pair repulsion model (Cl2−Sb1−S1A = 169.56° and Cl3−Sb1−S2B = 172.30° in **3** (Figure 5), Cl1−Sb1−Cl2 = 171.53° and S2A−Sb1−S2B = 174.86° in **4** (Figure 6), Cl2−Sb1−S2A = 168.51° and Cl1−Sb1−S2B = 169.11° in **5** (Figure 7), and Cl1−Sb1−Cl2 = 163.58° and S1A−Sb1−Cl3 = 176.57° in **6** (Figure 8)).

Furthermore, the water molecules cocrystallized, in the case of complexes **1** and **2** exhibiting Oh geometry, and are involved in hydrogen bonding (O1W···N31 = 2.825 Å, O1W···Cl1′= 3.257 Å, O1W−O2W = 2.762 Å, O1W···OW3 = 2.872 Å, O2W···S22 = 2.767 Å, and O2W···S32 = 2.784 Å, respectively, in **1** (Figure 3) and (O1W···N11 = 2.942 Å, O1W···N21 = 2.918 Å, O1W−Cl3 = 2.967 Å, and O2W···Cl2 = 3.253 Å, respectively, in **2** (Figure 4)), forming a three-dimensional (3D) network. Figure 9 shows the unit cell of complex **1**. In the case of complexes **3**−**6** with SP geometry, inter- and/or intramolecular hydrogen bonding and weak electrostatic interactions (e.g., S···N, Cl···S, or S···S, etc.) lead to supramolecular self-assemblies.[17b,c] Thus, in complexes with SP geometry, such bonding interactions are found to be N3B···S2A′ = 3.272 Å and S2A···Cl3 = 3.440 Å in **3** (Figure 5), N1A···Cl2 = 3.258 Å and S2A···Cl2′ = 3.448 Å in **4** (Figure 6), S2A···S1B′ = 3.349 Å and Cl1···N3A′ = 3.285 Å in **5** (Figure 7), and S2A···S1A′ = 3.580 Å and Cl1···N6A′ = 3.215 Å in the case of complex **6** (Figure 8) (the primary Sb atoms belong to a second molecule). The intermolecular Sb···S′ distances (the primary Sb atoms belong to a second molecule) in complexes **3**−**6** are found to be very long, confirming the monomeric structure of these complexes (Sb1···S2A′ = 5.869 Å and Sb1···S2A′ = 7.566 Å in **3**, Sb1···S2A′ = 16.737 Å and Sb1···S2A′ = 12.580 Å in **4**, Sb1···S2A′ = 5.546 Å and Sb1···S2A′ = 6.130 Å

(17) (a) Haiduc, I.; Silvestru, C. *Main Group Elements and Their Compounds*; Springer-Verlag: Berlin, 1996; p 355. (b) Liu, Y.; Tiekink, E. R. T. *CrystEngComm.* **2005**, *7*, 20−27. (c) Vickaryous, W. J.; Zakharov, L. N.; Johnson, D. W. *Main Group Chem.* **2006**, *5*, 51−59.

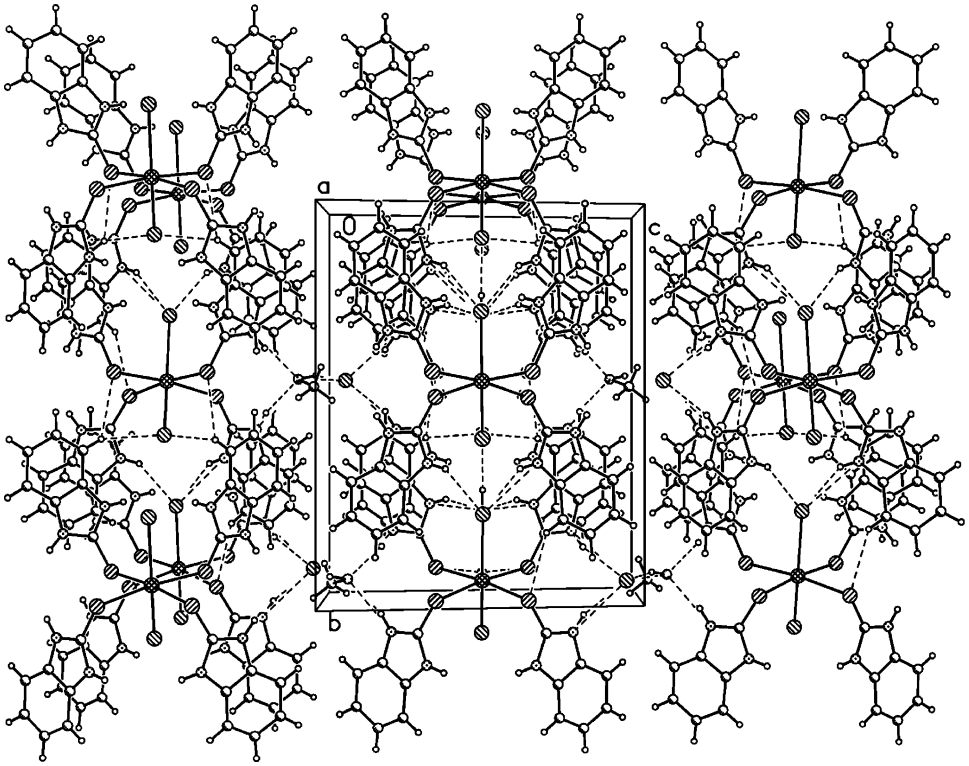

Figure 9. Unit cell of complex **1**. Stong hydrogen bonds result in a 3D network, which involves the water molecules that are cocrystallized.

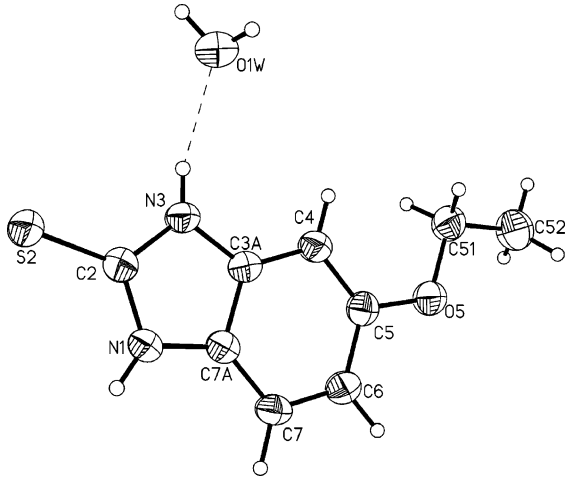

Figure 10. Anisotropic ellipsoid representation of ligand EtMBZIM·H_2O. The ellipsoids are drawn at the 50% probability level. Selected bond distances (Å) and angles (deg): S2−C2 = 1.691(3), N1−C2 = 1.350(3), N3−C2 = 1.350(3), N1−C7A = 1.388(3), N3−C3A = 1.395(3), O5−C5 = 1.386(3), O5−C51 = 1.438(3), S2−C2−N1 = 126.5(2), S2−C2−N3 = 126.1(2), N1−C2−N3 = 107.4(2), C7A−N1−C2−S2 = −177.7(2).

in **5** and Sb1···S2A′ = 9.711 Å and Sb1···S2A′ = 6.119 Å in **6** (Figures 5−8).

VI. Crystal and Molecular Structure of the Hydrated Ligand, EtMBZIM·H_2O. The ORTEP diagram of the EtMBZIM·H_2O ligand is shown in Figure 10. The C−S bond distance is 1.691(3) Å, indicating the thionate form of the ligand in solid state as expected for thione−thiol ligands[18a] and is in accordance with the corresponding bond distances found in 2-mercapto-benzimidazole (C−S = 1.670(3) Å),[18b] 2-mercapto-benzothiazole (C−S = 1.666(2) Å),[18c] or 2-mercapto-benzoxazole (C−S = 1.642(2) Å).[18d] This C−S bond distance is slightly lengthened upon coordination of EtMBZIM to Sb(III) cations (Table 1).

VII. X-ray Powder Diffraction Study. To examine further our hypothesis about the influence of water molecules in the geometry adopted by the Sb(III) complexes (see conductivity titration), we grew crystals of the ionic complex **2** from acetonitrile/water solutions. According to the thermal analysis results (see above), these water molecules are released when the samples of the ionic complexes are heated higher than 140 °C. Thus, by studying the X-ray powder diffraction (XRPD) diagrams of complex **1** before and after heating at 150 °C for 12 h (parts A and B of Figure 11) and by comparing the latter with the calculated X-ray diffraction data, the XRPD diagram of complex **3** (Figure 11C), we found that the XRPD diagrams of complexes **3** and **1** after heating at 150 °C for 12 h (parts B and C of Figure 11) were identical, leading to the conclusion that, in the solid state, the evolution of the water molecules from the ionic complex **1** causes the geometry transformation of the octahedral ionic complex **1** to the SP neutral complex **3**. Thus, water molecules play an important role in the geometry of the Sb(III) complexes adopted. Earlier, Giolando et al.[19] had described the influence of di-oxygen on the geometries of Sb(III) complexes. In this report, the treatment of $SbCl_3$ with the anion of benzene-1,2-dithiol (1,2-$MS_2C_6H_4$, M = Na or Li) results in the formation of M[Sb(1,2-$S_2C_6H_4)_x$] (x = 2 or 3) complexes. Thus, the {[Sb^{III}(1,2-$S_2C_6H_4)_2$]$^-$} anion,

(18) (a) Raper, E. S. *Coord. Chem. Rev.* **1985**, *61*, 115. (b) Form, G. R.; Raper, E. S.; Downie, T. C. *Acta Crystallogr., Sect. B* **1976**, *32* 345 (c) Radka, A. *Z. Kristallogr*. **1985**, *171*, 225. (d) Kubicki, M.; Hadjikakou, S. K.; Hadjiliadis, N., unpublished results.

(19) Wegener, J.; Kirschbaum, K.; Giolando, D. M. *J. Chem. Soc., Dalton Trans.* **1994**, 1213−1218.

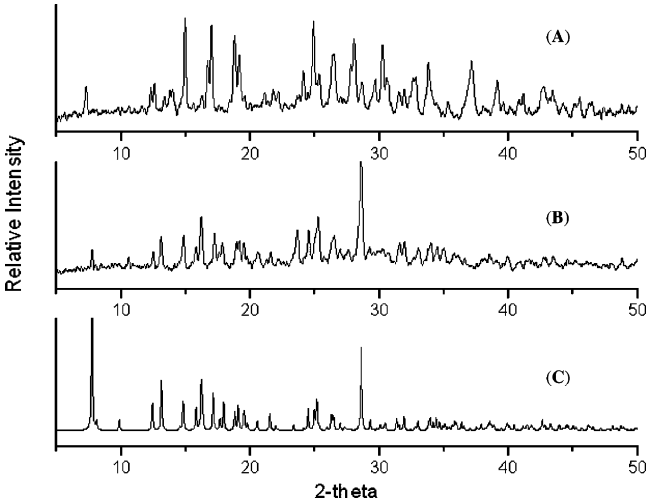

Figure 11. XRPD diagrams of complex **1** before and after heating at 150 °C for 12 h (A and B) and the calculated XRPD diagram of complex **3** (C).

Table 2. Inhibitory Effects of Antimony(III) Complexes on the Proliferation of Murine Leukemia Cells (L1210), Murine Mammary Carcinoma Cells (FM3A), Human T-lymphocyte Cells (Molt4/C8, CEM), and Human Cervix Carcinoma Cells (HeLa)

	IC_{50}[a] (μM)				
compound	L1210	FM3A	Molt4/C8	CEMt	Hela
1	12 ± 7	36 ± 6	24 ± 16	90 ± 19	6.4 ± 1.6
2	20 ± 15	88 ± 49	30 ± 21	88 ± 5	7.0 ± 2.0
3	31 ± 8	103 ± 44	45 ± 33	112 ± 6	7.7 ± 1.2
4	21 ± 16	41 ± 5	15 ± 10	24 ± 2	6.9 ± 1.1
5	29 ± 10	56 ± 7	32 ± 22	124 ± 8	6.8 ± 4.4
6	29 ± 12	92 ± 55	38 ± 7	118 ± 4	7.7 ± 2.5

[a] 50% inhibitory concentration.

with ψ-TBP geometry, precipitated from slowly cooling hot MeCN solutions under anaerobic conditions while the $\{[Sb^{V}(1,2\text{-}S_2C_6H_4)_3]^-\}$ complex with Oh geometry was derived from MeCN/MeOH solutions when aerobic conditions were employed for the reaction. Finally, $\{[Sb^{V}(1,2\text{-}S_2C_6H_4)_3]^-\}$ can be obtained from $\{[Sb^{III}(1,2\text{-}S_2C_6H_4)_2]^-\}$ with an excess of ligand and O_2. In our case, however, the reaction conditions were aerobic in all reactions studied.

VIII. Biological Tests. Antitumor Activity. Complexes **1**−**6** were tested in vitro for their inhibitory effects on the proliferation of murine leukemia cells (L1210), murine mammary carcinoma cells (FM3A), human T-lymphocyte cells (Molt4/C8, CEM), and human cervix carcinoma cells (HeLa). The results of this study are reported, as 50% inhibitory concentration (IC_{50}) values, in Table 2. Complexes **1**−**6** showed a pronounced cytostatic activity against the tumor cell lines studied (see Table 2). Surprisingly, antimony(III) thione complexes consistently showed selective antiproliferative activity against HeLa cells. Their antiproliferative activity against cervix carcinoma (HeLa) cells was 2−3- to >10-fold stronger than against the leukemia and lymphocyte cells. Complex **1** with Oh geometry exhibits a slightly stronger cytotoxicity against murine leukemia cells (L1210), murine mammary carcinoma cells (FM3A), and human cervix carcinoma cells (HeLa). Complex **4** with *trans*-a,b,c-Cl, *trans*-S, and SP geometry was more active against human T-lymphocyte cells (Molt4/C8, CEM) than the other complexes. The corresponding IC_{50} values found for cisplatin and carboplatin on the proliferation of HeLa cells are 10.1 and >37 μM respectively.[20a] Thus, all antimony(III) complexes **1**−**6** tested showed stronger activity against cancerous HeLa cells with the cytotoxicity of complex **1** 6 times higher than that of carboplatin.[20a] The IC_{50} values found for cisplatin on the proliferation of L1210/0 or Molt4 cells are 0.23 and 0.33 μM,[20b,c] respectively, indicating the low cytotoxic activity of the complexes **1**−**6** against these cell lines with respect to the corresponding activity of cisplatin. It would be of particular interest to evaluate the anti-leismanian activity for the compounds.

Scheme 3

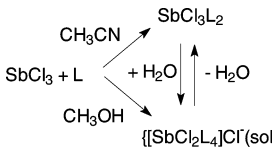

3. Conclusion

New antimony(III) complexes with the thiones 2-mercapto-benzimidazole (MBZIM), 5-ethoxy-2-mercapto-benzimidazole (EtMBZIM), 2-mercapto-thiazolidine (MTZD), and 2-mercapto-3,4,5,6-tetrahydro-pyrimidine (tHPMT), of Oh and SP structures were prepared and characterized crystalographically. The reaction of thiones with $SbCl_3$ under aerobic conditions results in the formation of complexes with structural diversity, with water as a solvent/ligand playing an important role in the determination of the final product. Thus, complexes derived from MeOH/H_2O solutions are ionic with an Oh geometry around the metal center $\{[SbL_4Cl_2]^+Cl^-(solv)\}$ (solv = $2H_2O{\cdot}CH_3OH$ in **1** or $3H_2O{\cdot}CH_3CN$ in **2**). When acetonitrile is used as a solvent for the conductivity titration, the neutral complexes of formula $\{[SbL_2Cl_3]\}$ (**3**−**6**) were obtained with SP geometries. The addition of water in the solvent media during the titration in acetonitrile leads to the formation of a high-conductance solution, as in the case of the ionic species. Thus, a geometry transition from an SP configuration to an Oh configuration may take place. Heating a solid sample of complex **1** at 150 °C, on the other hand, results in the evolution of a water molecule with a subsequent transition from the Oh conformation to the SP one, according to the XRPD diagrams.

These results led us to conclude that presence of water in the reaction of thiones with $SbCl_3$ strongly affects the geometry of the outcomes while the geometry transition may occur by the addition/substraction of water molecules (Scheme 3).

The complexes showed moderate cytostatic activity against several tumor cell lines with a preference for human cervix carcinoma (HeLa) cells.

(20) (a) Carland, M.; Tan, K. J.; White, J. M.; Stephenson, J.; Murray, V.; Denny, W. A.; McFadyen, D. *J. Inorg. Biochem.* **2005**, *99*, 1738−1743. (b) Shamsuddin, S.; Takahashi, I.; Siddik, Z. H.; Khokhar, A. R. *J. Inorg. Biochem.* **1996**, *61*, 291−301. (c) Dabholkar, M.; Parker, R.; Reed, E. *Mutat. Res. DNA Repair* **1992**, *274*, 45−56.

Table 3. Crystal Data and the Structure Refinement Details for the Complexes **1**−**6** and EtMBZIM·H_2O

	1	**2**	**3**	**4**	**5**	**6**	EtMBZIM·H_2O
empirical formula	$C_{29}H_{32}Cl_3N_8O_3S_4Sb$	$C_{28}H_{28}Cl_3N_8O_2S_4Sb$	$C_{14}H_{12}Cl_3N_4S_2Sb$	$C_{18}H_{20}Cl_3N_4O_2S_2Sb$	$C_6H_{10}Cl_3N_2S_4Sb$	$C_8H_{16}Cl_3N_4S_2Sb$	$C_9H_{12}N_2O_2S$
formula weight	896.928	864.895	528.494	616.582	466.498	460.456	212.244
T (K)	293	293	293	293	293	293	293
cryst syst	monoclinic	monoclinic	triclinic	triclinic	monoclinic	triclinic	triclinic
space group	$P2_1$	$P2_1$	$P\bar{1}$	$P\bar{1}$	$P2_1/c$	$P\bar{1}$	$P\bar{1}$
a (Å)	7.7398(8)	7.8216(8)	7.3034(5)	8.6682(6)	8.3659(10)	7.4975(6)	7.4539(8)
b (Å)	16.724(3)	16.7426 (17)	11.2277(7)	10.6005(7)	14.8323(19)	10.3220(7)	8.5110(12)
c (Å)	13.717(2)	13.9375(16)	12.0172(8)	13.0177(9)	12.0218(13)	12.1094(11)	9.4913(8)
α (deg)	90.00	90.00	76.772(5)	84.181(6)	90.00	71.411(7)	71.182(10)
β (deg)	98.632(11)	99.218(10)	77.101(6)	79.358(6)	99.660(12)	84.244(7)	72.305(9)
γ (deg)	90.00	90.00	87.450(5)	84.882(6)	90.00	73.588(6)	66.357(12)
V (Å^3)	1755.4(4)	1801.6 (3)	935.04(11)	1166.49(14)	1470.6(3)	852.00(13)	511.41(11)
Z	2	2	2	2	4	2	2
ρ_{calcd} (g/cm^3)	1.697	1.5860	1.877	1.756	2.107	1.795	1.300
μ (mm^{-1})	1.30	1.26	2.1	1.7	3.0	2.3	0.3
R, wR2 [$I > 2\sigma(I)$]	0.0994, 0.2602	0.0744, 0.1835	0.0272, 0.0712	0.0270, 0.0601	0.0598, 0.1209	0.0189, 0.0470	0.0312, 0.0948

4. Experimental Section

Materials and Instruments. All solvents used were of reagent grade. Antimony(III) chloride (Fluka) as well as thiones 2-mercapto-benzimidazole, 5-ethoxy-2-mercapto-benzimidazole, 2-mercapto-thiazolidine, and 2-mercapto-3,4,5,6-tetrahydro-pyrimidine (Aldrich) were used without further purification. Elemental analyses for C, H, N, and S were carried out with a Carlo Erba EA MODEL 1108 elemental analyzer. Infrared spectra in the region of 4000−370 cm^{-1} were obtained in KBr pellets while far-infrared spectra in the region of 400−50 cm^{-1} were obtained in polyethylene discs, with a Perkin-Elmer Spectrum GX FT-IR spectrometer. Micro FT-Raman measurements were carried out using near-infrared laser radiation (Nd^{3+}: YAG, 1064.1 nm). FT-Raman spectra (2.6 cm^{-1} resolution) were recorded on a Bruker IFS-88 FT-IR/FRA-105 Raman module fitted with a Ge proprietary detector and coupled via two 1.0 m photooptic cables to a Nikon Optiphot-II optical microscope equipped with a Nikon 20×, super-long-range objective lens. Near-IR laser radiation was directed onto the sample through the objective and collected along the same optical pathway in a 180° backscattering mode. Samples were measured as solid powders dispersed on a glass slide. Thermal studies were carried out on a Shimadzu DTG-60 simultaneous DTA-TG apparatus, under a N_2 flow (50 cm^3 min^{-1}) with a heating rate of 10 °C min^{-1}. Conductivity titrations were carried out at T = 293 K in methanol and acetonitrile or acetonitrile/water solutions with a WTF LF-91 conductivity meter.

Synthesis and Crystallization of {$[SbCl_2(MBZIM)_4]^+\cdot Cl^-\cdot 2H_2O\cdot(CH_3OH)$} (1), {$[SbCl_2(MBZIM)_4]^+\cdot Cl^-\cdot 3H_2O\cdot(CH_3CN)$} (2), $[SbCl_3(MBZIM)_2]$ (3), $[SbCl_3(EtMBZIM)_2]$ (4), $[SbCl_3(MTZD)_2]$ (5), and $[SbCl_3(tHPMT)_2]$ (6) Complexes. Measures of 0.5 mmol of the appropriate thiones of 2-mercapto-benzimidazole (0.075 g), 5-ethoxy-2-mercaptobenzimidazole (0.097 g), 2-mercapto-thiazolidine (0.059 g), and 3,4,5,6-tetrahydro-2-mercapto-pyrimidine (0.058 g) were dissolved in dichloromethane (10 cm^3). A solution of antimony(III) chloride (0.114 g, 0.5 mmol) in methanol (10 cm^3) for complex **1**, in acetonitrile (10 cm^3) with a few drops of water for complex **2**, or dichloromethane (10 cm^3) for complexes **3**, **5**, and **6** was then added to the above solution. In the case of complex **4**, 1 mmol of antimony(III) chloride (0.228 g) in dichloromethane (10 cm^3) was used. The solutions of complexes **1** and **2** were filtered off, and the resulting clear solutions were kept in darkness at room temperature to give crystals of the named complexes **1** and **2**. In the case of complexes **3**−**6**, the solutions were stirred for 15 min and the resulting precipitations were filtered off and dried. Recrystallization of these solids with hot CH_3CN (20 cm^3) yields crystals of complexes **2**−**6**. All solid products are stable when kept in darkness at room temperature. Complexes **1**−**4** are soluble in methanol, acetone, acetonitrile, DMSO, and DMF. Complex **5** is soluble in acetone, MeCN, DMSO, and DMF while **6** is soluble only in DMSO and DMF.

Results for **1**: orange crystals; yield 38%; mw, 915.01 g/mol. Elemental analyses, Found: C, 38.16; H, 3.50; N, 12.44; S, 13.95. Anal. Calcd for $C_{29}H_{32}Cl_3N_8O_3S_4Sb$: C, 38.83; H, 3.59; N, 12.49; S, 14.30. IR (cm^{-1}): 3064m, 1618m, 1492s, 1450s, 1389w, 1365w, 1348s, 1249w, 1222w, 1164m, 1011m, 975m, 753s, 740s, 619w, 600s, 460w.

Results for **2**: orange crystals; yield 25%; mw, 861.932 g/mol. Elemental analyses, Found: C, 39.02; H, 3.42; N, 12.75; S, 14.95. Anal. Calcd for $C_{28}H_{28}Cl_3N_8O_2S_4Sb$: C, 38.88; H, 3.26; N, 12.95; S, 14.83. IR (cm^{-1}): 3069m, 1618s, 1498s, 1451s, 1389w, 1349s, 1257w, 1221w, 1174m, 1007w, 973m, 859w, 746s, 619w, 601s, 470w.

Results for **3**: yellow crystals; yield 30%; mw, 525.861 g/mol. Elemental analyses, Found: C, 31.64; H, 2.40; N, 10.45; S, 11.99. Anal. Calcd for $C_{14}H_{12}Cl_3N_4S_2Sb$: C, 31.82; H, 2.29; N, 10.60; S, 12.13. IR (cm^{-1}): 3098m, 1622s, 1508s, 1459s, 1392m, 1346s, 1254m, 1211w, 1170s, 1013w, 979m, 938w, 739s, 602s, 473m, 463w.

Results for **4**: brown crystals; yield 35%; mw, 616.63 g/mol. Elemental analyses, Found: C, 35.66; H, 3.40; N, 9.32; S, 10.55. Anal. Calcd for $C_{18}H_{20}Cl_3N_4O_2S_2Sb$: C, 35.06; H, 3.27; N, 9.09; S, 10.40. IR (cm^{-1}): 3200m, 2974w, 1631s, 1491s, 1458s, 1397w, 1336w, 1304s, 1261w, 1228w, 1184w, 1167m, 1124m, 1042m, 983w, 966w, 906w, 823s, 694m, 660m, 623m, 579m, 522w.

Results for **5**: yellow crystals; yield 45%; mw, 466.54 g/mol. Elemental analyses, Found: C, 15.75; H, 2.04; N, 5.86; S, 27.60. Anal. Calcd for $C_6H_{10}Cl_3N_2S_4Sb$: C, 15.45; H, 2.16; N, 6.00; S, 27.49. IR (cm^{-1}): 3274m, 1520s, 1459m, 1342w, 1306s, 1249w, 1192w, 1044s, 993s, 928m, 628m, 557m, 539w.

Results for **6**: yellow crystals; yield 43%; mw, 460.49 g/mol. Elemental analyses, Found: C, 21.02; H, 3.44; N, 12.50; S, 14.03. Anal Calcd for $C_8H_{16}Cl_3N_4S_2Sb$: C, 20.87; H, 3.50; N, 12.17; S, 13.93. IR (cm^{-1}): 3212m, 3151m, 2970m, 2870w, 1618s, 1577s, 1561s, 1471w, 1432m, 1361s, 1346w, 1314s, 1278w, 1232m, 1201m, 1073m, 981w, 939w, 866w, 814m, 730m, 634m, 558m, 519w.

X-ray Structure Determination. Intensity data for the colorless crystals of **1**−**5** were collected on a KUMA KM4CCD four-circle diffractometer[21a] with a CCD detector, using graphite-monochro-

mated Mo Kα radiation ($\lambda = 0.71073$ Å). Cell parameters were determined by a least-squares fit.[21b] All data were corrected for Lorentz-polarization effects and absorption.[21b]

The structures were solved with direct methods with *SHELXS97*[21c] and refined by full-matrix least-squares procedures on F^2 with *SHELXL97*.[21d] All non-hydrogen atoms were refined anisotropically, hydrogen atoms were located at calculated positions and refined via the "riding model" with isotropic thermal parameters fixed at 1.2 (1.3 for CH_3 groups) times the U_{eq} value of the appropriate carrier atom. Significant crystal data are given in Table 3.

Supplementary data are available from the CCDC, 12 Union Road, Cambridge CB2 1EZ, U.K., (e-mail: deposit@ccdc.cam.ac.uk), on request, quoting the deposition nos. CCDC 642873 and 642874 for complexes **1** and **2**, respectively, and CCDC 642434−642438 for complexes **3**−**6** as well as EtMBZIM H_2O, respectively.

X-ray Powder Diffraction. X-ray powder diffraction patterns, from the powder derived from crystals, were obtained using a Bruker AXS D8 Avance diffractometer in Bragg−Brentano geometry equipped with a Cu sealed-tube radiation source ($\lambda = 1.54178$ Å) and a secondary beam graphite monochromator. The generator was set to 40 kV and 40 mA. The 2θ range used in the measurements was from 5° to 50° in steps of 0.02° with a count time of 10 s per step.

Cytostatic Activity Assays. Murine leukemia L1210, murine mammary carcinoma FM3A, human T-lymphocyte Molt 4 and CEM, and human cervix carcinoma HeLa cells were suspended at 300,000−500,000 cells/mL in a culture medium, and 100 μL of a cell suspension was added to 100 μL of an appropriate dilution of the test compounds in a 96-well microtiter plates apparatus. After incubation at 37 °C for 2 (L1210 and FM3A) or 3 (Molt4, CEM and HeLa) days, the cell number was determined using a Coulter counter. The number of the suspension cells was counted directly; the number of the monolayer HeLa cells was counted after detachment of the cells upon trypsinization. The IC_{50} level was defined as the compound concentration required to inhibit cell proliferation by 50%.

Acknowledgment. This research was carried out in partial fulfillment of the requirements for the Ph.D. thesis of I.I.O. within the graduate program in Bioinorganic Chemistry, coordinated by N.H. N.H and I.S.B would like to thank a NATO grant for the exchange of scientists. I.I.O. would like to thank the Hellenic Ministry of Education for a scholarship for postgraduate studes.

IC700756E

(21) (a) *CrysAlis CCD*, version 1.171.31.5 (release 28-08-2006 CrysAlis171.NET); Oxford Diffraction, Ltd. (b) *CrysAlis RED*, version 1.171.31.5 (release 28-08-2006 CrysAlis171.NET); Oxford Diffraction, Ltd. (c) Sheldrick, G. M. *Acta Crystallogr.* **1990**, *A46*, 467. (d) Sheldrick, G. M. *SHELXL-97, Program for the Refinement of Crystal Structures*; University of Göttingen: Göttingen, Germany, 1997.